ISSN: 2414-1895 DOI: 10.6919/ICJE.202506_11(6).0018

Spiral-Encoded Illumination for Robust Phase-Amplitude Recovery in Fourier Ptychographic Microscopy

Boyu Yang[1], Xingbo Zhu[1], Fangyuan Yao[2], Zonglin Li[1]

[1] North China University of Science and Technology, Tangshan, 063000, China

[2] Zhangjiakou University, Zhangjiakou, 075000, China

Abstract

Fourier Ptychographic Microscopy (FPM) is a computational imaging technique that reconstructs high-resolution phase and amplitude images from low-resolution intensity measurements. This study presents a robust FPM reconstruction framework based on spiral-encoded LED illumination and an iterative Gerchberg–Saxton algorithm with frequency-domain error feedback. A complex object combining amplitude and phase components is synthesized to simulate realistic samples. A total of 255 low-resolution images are generated using a 15×15 spiral LED array. The reconstruction iteratively updates the object's spectrum with amplitude constraints guided by phase retrieval error. Experimental results show that the proposed method achieves a PSNR of 37.33 dB and SSIM of 0.9848 for amplitude, and a PSNR of 24.18 dB and SSIM of 0.9384 for phase, demonstrating its effectiveness for high-fidelity phase-amplitude recovery in FPM.

Keywords

Fourier Ptychographic Microscopy; Spiral Illumination; Phase Retrieval; Gerchberg–Saxton Algorithm; Frequency-Domain Reconstruction; Computational Imaging; Error Feedback.

1. Introduction

With the rapid development of digital pathology, live-cell monitoring, drug screening, and histopathological imaging, there is an increasing demand for biomedical imaging modalities that offer high resolution, large field of view (FOV), non-invasive acquisition, and system stability simultaneously [1–3]. However, traditional optical microscopes are fundamentally constrained by the diffraction limit, which is governed by the numerical aperture (NA) of the objective lens and the wavelength of illumination [4]. Moreover, these systems typically provide a limited FOV, making them inefficient for imaging large biological specimens. Although increasing the NA can enhance resolution, it inevitably reduces the FOV and depth of field, while also escalating system cost and complexity [5], resulting in the well-known trade-off between resolution and FOV.

Fourier ptychographic microscopy (FPM), a computational optical imaging technique, offers a compelling solution to this dilemma by integrating low-NA illumination with frequency domain stitching to achieve super-resolution imaging without altering hardware complexity [6–8]. The core principle involves illuminating the sample from multiple oblique angles using a programmable LED array, capturing a series of low-resolution intensity images, and reconstructing a high-resolution complex image through iterative phase retrieval and frequency domain synthesis [9]. Since FPM relies solely on a low-NA objective and an LED array, it eliminates the need for expensive optics or mechanical scanning, making it highly accessible, scalable, and consistent for various imaging tasks [10].

ISSN: 2414-1895 DOI: 10.6919/ICJE.202506_11(6).0018

Despite its theoretical elegance and experimental effectiveness, FPM still faces several practical challenges that hinder its broader application. First, non-uniform angular distribution and intensity inconsistency of the LED array can lead to uneven overlap in the frequency domain, resulting in coverage gaps or redundancies that severely degrade edge detail restoration [11,12]. Second, conventional phase retrieval algorithms such as the Gerchberg–Saxton (G-S) scheme are highly sensitive to initialization and noise, often producing local minima or artifact propagation-particularly problematic in low-SNR biomedical scenarios [13]. Third, system-induced errors such as LED misalignment, illumination instability, and sensor response non-uniformity are difficult to model and correct within standard FPM algorithms, limiting their repeatability and clinical reliability [14,15].

To address these issues, recent efforts have focused on optimizing illumination strategies and reconstruction algorithms in FPM. For instance, Zhou et al. proposed a fast FPM reconstruction framework based on spatial frequency fusion, employing window functions to improve spectrum stitching efficiency [16]. Chen et al. introduced deep neural network-based enhancement modules to compensate for high-frequency losses and suppress reconstruction artifacts [17,18]. Zhang et al. developed a residual channel attention network to better extract edge and textural features [19]. However, these approaches still suffer from several limitations: (1) the spectral fusion strategies are not generally adaptive and lack robustness to variations in sample structure and system state; (2) error propagation mechanisms are not explicitly modeled, making the reconstruction process sensitive to early-stage errors; (3) existing deep-learning-based methods do not incorporate sufficient physical constraints on the phase retrieval process, reducing their generalizability to deeper tissues or larger FOVs [20–22].

To improve frequency-domain sampling uniformity and enhance reconstruction stability, this paper presents a Fourier ptychographic reconstruction framework based on a spiral-encoded LED illumination sequence. A 15×15 LED array is programmed to follow a spatially continuous spiral scanning pattern, enabling consistent and dense coverage of the spatial frequency domain. During reconstruction, a standard Gerchberg–Saxton (G-S) iterative algorithm is employed to update the complex object spectrum. In each iteration, the simulated low-resolution image amplitude is enforced while the phase is preserved, facilitating spectral refinement via frequency-domain error feedback. A multi-metric evaluation scheme is introduced, incorporating amplitude error (EA), phase error (EP), and total reconstruction error (E), to monitor convergence trends and assess reconstruction stability throughout the iterative process.

The proposed method is validated using synthetic data. A complex-valued object is generated by combining a 400×400 high-resolution amplitude image and phase map. A total of 255 low-resolution intensity images are simulated using the spiral illumination pattern. The reconstruction is performed over 10 iterations, and the results are quantitatively assessed using PSNR, SSIM, and visual error maps. The reconstructed amplitude image achieves a PSNR of 37.33 dB and SSIM of 0.9848, while the phase image reaches a PSNR of 24.18 dB and SSIM of 0.9384. These results demonstrate that the proposed illumination strategy and error-guided iterative framework can achieve high-fidelity joint recovery of amplitude and phase without prior constraints.

The main contributions of this work are summarized as follows:(1) A spiral-encoded LED illumination strategy is proposed to ensure continuous and consistent sampling in the frequency domain, improving sub-spectrum alignment;(2) A frequency-domain iterative reconstruction framework is developed based on amplitude enforcement and error feedback, enabling high-accuracy phase-amplitude recovery without supervision;(3) A three-metric error evaluation scheme is introduced to quantitatively assess convergence behavior and provide a foundation for future adaptive error control mechanisms.

2. Methodology

To achieve high-fidelity phase and amplitude reconstruction, we construct a frequency-domain computational imaging framework tailored for FPM. The entire pipeline spans from acquisition-side

Volume 11 Issue 6, 2025
DOI: 10.6919/ICJE.202506_11(6).0018

spiral LED illumination to reconstruction-side spectral fusion and error-guided optimization. To provide an overview of the complete system architecture, Section 2.1 introduces a system-level schematic. Subsequent sections elaborate on each module, including object modeling, illumination mapping, image synthesis, and iterative reconstruction.

2.1 System Architecture Overview

Figure 1 presents the schematic diagram of the proposed Fourier ptychographic microscopy system. The system consists of three core components: (1) a 15×15 spiral-encoded LED array that enables angularly diverse illumination; (2) a CMOS or CCD-based sensor responsible for capturing low-resolution intensity images; and (3) a reconstruction module based on frequency-domain Gerchberg–Saxton iteration. In this study, synthetic complex objects with both amplitude and phase features are constructed, and a sequence of 255 low-resolution images is generated by simulating spiral illumination under the physical imaging model. These frames are then processed by the iterative reconstruction algorithm to recover a high-resolution complex object comprising both amplitude and phase.

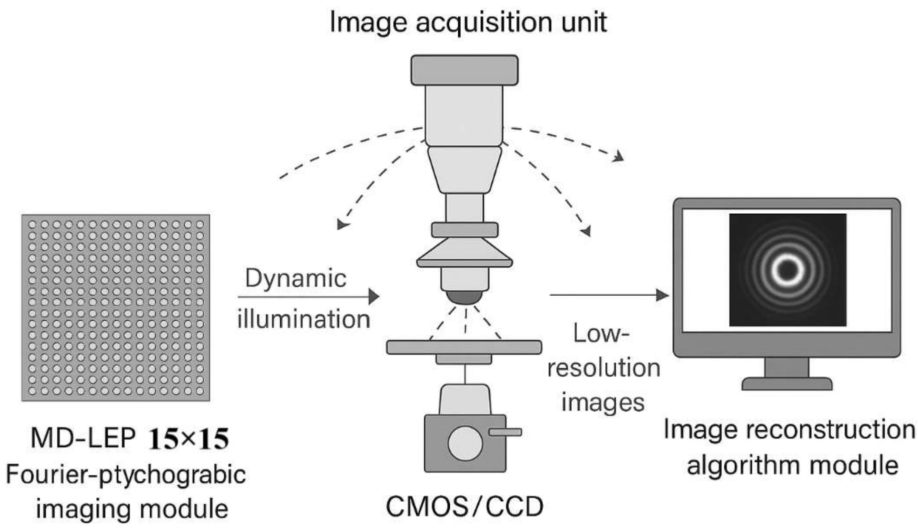

Figure 1. Schematic diagram of the Fourier ptychographic imaging system.

From left to right: a 15×15 spiral LED array (MD-LEP), a low-resolution image acquisition unit (CMOS or CCD sensor), and a frequency-domain reconstruction module. The system sequentially illuminates the sample at different incident angles and collects corresponding intensity images, which are jointly used to reconstruct the high-resolution amplitude and phase distribution of the sample.

2.2 Object Modeling

To simulate a complex imaging target with both amplitude and phase modulation, we construct a two-dimensional synthetic complex-valued object, which serves as the ground truth reference for spectrum slicing, low-resolution synthesis, and reconstruction evaluation. The object is mathematically formulated as:

$$O(x, y) = A(x, y) \cdot exp\,[i \cdot \phi(x, y)] \tag{1}$$

Here, O(x, y) denotes the complex-valued object in the spatial domain, A(x, y) is the normalized amplitude map, and φ(x, y) is the phase distribution. The amplitude image is derived from

ISSN: 2414-1895 DOI: 10.6919/ICJE.202506_11(6).0018

cameraman.tif and processed via normalization and square root transformation to simulate optical absorption intensity. The phase image is taken from westconcordorthophoto.png, linearly normalized to the [0, 1] range to represent continuous phase modulation. Both components are resampled to a resolution of 400×400 pixels and aligned using bilinear interpolation to ensure pixel-level correspondence.

The final complex object is shown in Figure 2, where the left panel displays the amplitude distribution in grayscale, and the right panel shows the phase map, also rendered in grayscale for visualization purposes. Note that the phase map represents the wrapped phase values within [−π, π], and although visualized as a grayscale image, the original complex-valued phase information is fully preserved for subsequent processing. This object is used throughout the following simulation steps, including low-resolution image generation, reconstruction evaluation, and error metric computation.

(a) Amplitude map

(b) Phase map (grayscale visualization of wrapped phase in [−π, π])

Figure 2. Amplitude (left) and phase (right) maps of the simulated complex object.

2.3 Object Modeling

To achieve continuous and evenly distributed coverage in the spatial frequency domain, we adopt a spiral-encoded LED illumination strategy. The LED array is configured as an N × N grid, where N = 15. A spiral expansion algorithm is used to define a sequential illumination order seq(k), where each LED index $k \in [1, N^2]$ corresponds to a unique spatial position (x_i, y_i) in the array.

In the Fourier domain, each LED illumination introduces a spatial frequency shift corresponding to the incident angle of the light. Assuming that the LED plane is placed at a vertical distance h above the sample, the frequency offset is computed using a geometric projection model as:

$$k_x = \frac{x_0 - x_i}{\sqrt{(x_0 - x_i)^2 + (y_0 - y_i)^2 + h^2}}, k_y = \frac{y_0 - y_i}{\sqrt{(x_0 - x_i)^2 + (y_0 - y_i)^2 + h^2}} \tag{2}$$

Here, (x_0, y_0) denotes the center of the LED array, (x_i, y_i) is the spatial coordinate of the k^{th} LED, and h is the vertical distance from the LED array to the sample surface, which is set to 90 mm in this study. These frequency offsets (k_x, k_y) are directly mapped to the center positions of the sub-spectra in Fourier space.

By employing a center-outward spiral illumination pattern, the system ensures a progressive angular transition from low to high obliquity, thereby reducing nonuniform spectral sampling and improving sub-spectrum alignment stability during the reconstruction process.

ISSN: 2414-1895 DOI: 10.6919/ICJE.202506_11(6).0018

2.4 Low-Resolution Image Synthesis

According to the theory of Fourier optics, the low-resolution images captured under different illumination angles in FPM systems are equivalent to spatially low-pass filtered regions of the complex object's frequency spectrum. Specifically, for the k-th illumination direction, the simulated low-resolution image can be expressed as:

$$I_{low}^{(k)}(x,y) = |F^{-1}\{O_{FT}(k_x,k_y)\cdot CTF(k_x-k_{xc}^{(k)},k_y-k_{yc}^{(k)})\}|^2 \tag{3}$$

Here, F^{-1} denotes the 2D inverse Fourier transform, $O_{FT}(k_x, k_y)$ is the Fourier spectrum of the complex object $O(x, y)$; $(k_{xc}^{(k)}, k_{yc}^{(k)})$ represents frequency center shift induced by the k-th LED illumination; and $CTF(k_x, k_y)$ is the circular coherent transfer function defined as:

$$CTF(k_x,k_y) = \begin{cases} 1, & \sqrt{k_x^2+k_y^2} \le k_c \\ 0, & otherwise \end{cases} \tag{4}$$

The cutoff frequency $k_c = NA / \lambda$ is determined by the system's numerical aperture (NA) and the central wavelength $\lambda = 0.63$ μm.

In the simulation, for each illumination index seq(k), a square spectral region centered at $(k_{xc}^{(k)}, k_{yc}^{(k)})$ is extracted from the object's global spectrum, filtered by the ideal CTF, and inverse Fourier transformed to generate an intensity image. A total of 255 low-resolution frames are synthesized, which serve as the input dataset for the subsequent reconstruction algorithm.

2.5 Error-Driven Frequency-Domain Reconstruction

In the reconstruction stage, a classic Gerchberg–Saxton (G-S) iterative algorithm is employed to progressively update the global spectrum of the complex object in the frequency domain, enabling joint recovery of amplitude and phase. The initial state is set as a uniform complex field, represented in the Fourier domain by an all-ones matrix. In each iteration, following the spiral illumination sequence, the algorithm performs the following update steps for every frame:

First, a square sub-spectrum $\hat{o}_k^{(t)}$ centered at$(k_{xc}^{(k)}, k_{yc}^{(k)})$ is extracted from the current estimate $\hat{o}_{FT}^{(t)}$, and multiplied by the ideal CTF to simulate the system's optical bandwidth. The sub-spectrum is inverse Fourier transformed to obtain the estimated low-resolution image $I_k^{(t)}(x, y)$. Its amplitude is replaced by the square root of the simulated intensity $I_k(x, y)$, while its phase is preserved, yielding the corrected complex image:

$$\breve{I}_k^{(t)}(x,y) = \sqrt{I_k(x,y)}\cdot exp\left[i\cdot\angle\hat{I}_k^{(t)}(x,y)\right] \tag{5}$$

This image is then transformed back to the frequency domain to yield an updated sub-spectrum $\hat{o}_k^{'(t)}$, and the global spectrum is updated via:

$$\hat{O}_{FT}^{(t+1)} = \hat{O}_{FT}^{(t)} + \alpha\cdot\left(\hat{O}_k^{'(t)} - \hat{O}_k^{(t)}\right) \tag{6}$$

Here, $\alpha = 0.5$ is the spectral fusion coefficient, and $\hat{o}_{FT}^{(t)}$ denotes the global spectrum estimate at the t-th iteration.

ISSN: 2414-1895 DOI: 10.6919/ICJE.202506_11(6).0018

To assess reconstruction accuracy and convergence behavior, three error metrics are computed after each iteration:

Amplitude Error (EA):

$$\mathrm{EA}^{(t)} = \frac{\| A_{\mathrm{GT}} - A_{\mathrm{REC}}^{(t)} \|_2}{\| A_{\mathrm{GT}} \|_2} \tag{7}$$

Phase Error (EP):

$$\mathrm{EP}^{(t)} = \frac{\| \phi_{\mathrm{GT}} - \phi_{\mathrm{REC}}^{(t)} \|_2}{\| \phi_{\mathrm{GT}} \|_2} \tag{8}$$

Total Residual Error (E):

$$E^{(t)} = \frac{1}{K}\sum_{k=1}^{K} \frac{\| I_k - |\hat{I}_k^{(t)}|^2 \|_2}{\| I_k \|_2} \tag{9}$$

Here, A_{GT} and φ_{GT} represent the ground truth amplitude and phase, A_{REC} and φ_{REC} are the reconstructed results, and K = 255 is the total number of frames. These metrics are plotted over iterations and used in quantitative comparison to evaluate the algorithm's reconstruction fidelity and robustness.

3. Experiments and Results

To evaluate the contribution of the proposed spiral-encoded LED illumination strategy to reconstruction quality, we first conduct a comparative experiment across four illumination patterns-linear, diagonal, bidirectional, and spiral. Under identical simulation settings, each strategy is applied to reconstruct the same complex object, and the resulting amplitude and phase maps are evaluated using quantitative metrics such as PSNR (Peak Signal-to-Noise Ratio) and SSIM (Structural Similarity Index), revealing the impact of sampling uniformity on final reconstruction fidelity.

Subsequently, we implement a complete Fourier ptychographic simulation pipeline in MATLAB, including complex object generation, low-resolution image synthesis (255 frames), spectral stitching, and iterative reconstruction based on the Gerchberg–Saxton algorithm. To assess algorithmic convergence and robustness, three error metrics-Amplitude Error (EA), Phase Error (EP), and Global Residual Error (E)-are computed and tracked across iterations. All experiments are conducted under fixed parameters and controlled noise conditions to ensure reproducibility and fair comparison.

3.1 Experimental Setup

All experiments were conducted on the MATLAB R2023b simulation platform, using custom-developed routines for image processing and Fourier domain operations. The illumination system consists of a 15×15 LED array, totaling 255 illumination angles, with a spiral-encoded activation order. The vertical distance between the LED array and the object plane is set to h=90mm. The simulated complex object spans an area of 400×400 pixels in the sample plane. The imaging system uses a 4× objective lens with a numerical aperture (NA) of 0.1, and the illumination wavelength is set to λ=0.63μm.

For low-resolution image synthesis, the object spectrum is filtered using a circular coherent transfer function (CTF), and inverse Fourier transformed to generate 255 intensity images. Each image has a

ISSN: 2414-1895 DOI: 10.6919/ICJE.202506_11(6).0018

resolution of 1200×1600 pixels, simulating low-frequency observations of the same high-resolution object under varying illumination directions.

During reconstruction, the algorithm initializes with a uniform complex field in the frequency domain and updates the spectrum using the G–S iterative method. The spectral blending coefficient α is set to 0.5. In each iteration, all 255 frames are sequentially processed, and the algorithm is allowed to run for a maximum of 10 iterations. The reconstructed amplitude and phase maps are quantitatively compared with the ground truth using PSNR, SSIM, and residual error metrics.

3.2 Illumination Strategy Comparison

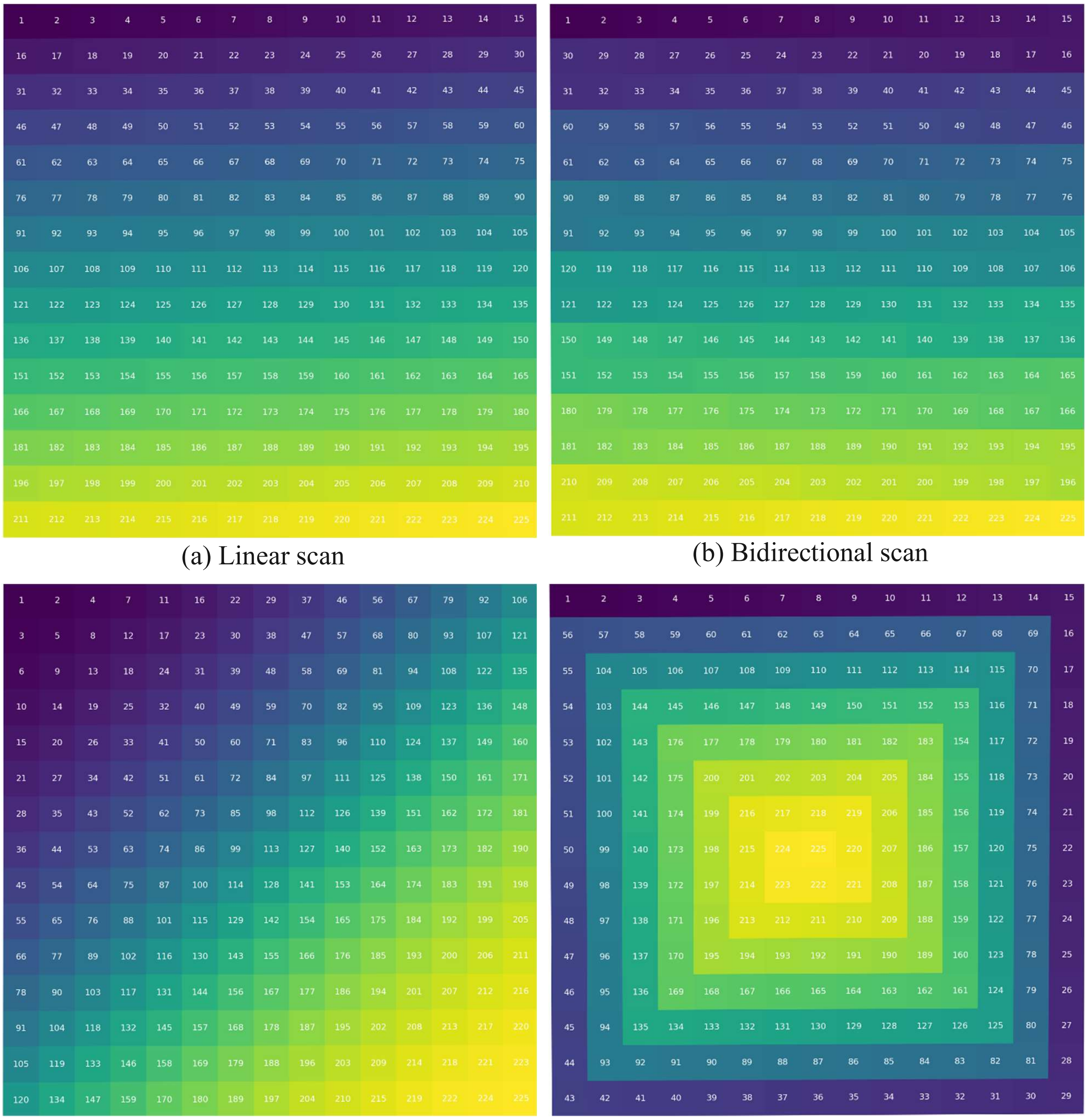

(a) Linear scan (b) Bidirectional scan

(c) Diagonal scan (d) Spiral scan (proposed)

Figure 3. Schematic illustrations of four LED illumination scheduling strategies.

To verify the rationality and effectiveness of selecting spiral-encoded illumination as the default scheduling strategy in our reconstruction framework, we compare it against three representative baselines: linear scan, diagonal traversal, and bidirectional sweep. Under consistent system

ISSN: 2414-1895 DOI: 10.6919/ICJE.202506_11(6).0018

configurations, we reconstruct the same complex object and evaluate the resulting image quality using PSNR and SSIM metrics. The comparison further validates the choice of spiral illumination from the perspectives of frequency-domain sampling uniformity and spectral stitching stability.

Figure 3 illustrates the spatial activation sequences of the four compared illumination strategies.

Table 1 presents the PSNR and SSIM values for both amplitude and phase reconstructions under each strategy.

Table 1. Reconstruction performance under different illumination strategies

Illumination Strategy	Amplitude PSNR (dB)	Amplitude SSIM	Phase PSNR (dB)	Phase SSIM
Linear	22.54	0.7147	12.77	0.1851
Bidirectional	37.11	0.9847	23.90	0.9364
Diagonal	37.12	0.9846	23.30	0.9392
Spiral(Ours)	**37.33**	**0.9848**	**24.18**	**0.9384**

The results clearly show that the linear scanning strategy suffers from highly non-uniform frequency coverage, leading to poor spectrum stitching and significant degradation in phase reconstruction (PSNR: 12.77 dB; SSIM: 0.1851). In contrast, all non-linear strategies demonstrate superior performance. Among them, the proposed spiral illumination yields the highest phase PSNR (24.18 dB), highlighting its advantage in enhancing spectral consistency and reconstruction fidelity.

3.3 Convergence and Error Curves

To assess the stability and convergence behavior of the proposed reconstruction framework, we monitor three complementary error metrics over 10 iterations: EA, EP, and E. These metrics collectively reflect the fidelity of both local feature recovery and global spectral alignment.

As illustrated in Figure 4, all three errors demonstrate clear convergence within the initial five iterations. The EA drops sharply from 0.032 to below 0.02 and remains stable afterward. The EP gradually increases and stabilizes around 0.213, indicating consistent phase mapping with negligible oscillation. Meanwhile, the E declines rapidly from 0.25 to below 0.01, reflecting robust spectral consistency under spiral illumination.

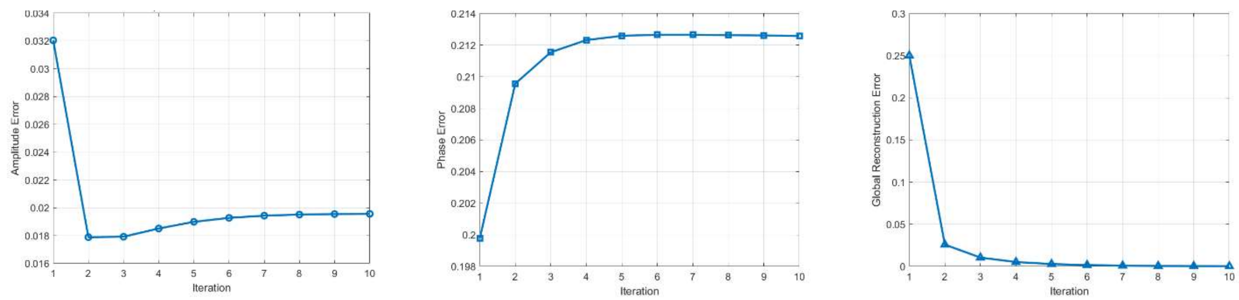

(a) Amplitude error (b) Phase error (c) Global residual error

Figure 4. Convergence curves of reconstruction errors over 10 iterations

These results confirm that the G–S iteration guided by error feedback and spiral-encoded illumination achieves fast, smooth, and reliable convergence, without suffering from local divergence or instability.

3.4 Reconstruction Error Map Analysis

To visualize the spatial accuracy of amplitude and phase reconstructions, we compare the ground truth and reconstructed results through pixel-wise difference and error maps. As shown in Figure 5,

Volume 11 Issue 6, 2025
DOI: 10.6919/ICJE.202506_11(6).0018

the first row presents amplitude-related results: (a) ground truth, (b) reconstruction, (c) signed amplitude difference map, and (d) enhanced error heatmap. The second row follows the same structure for phase reconstructions.

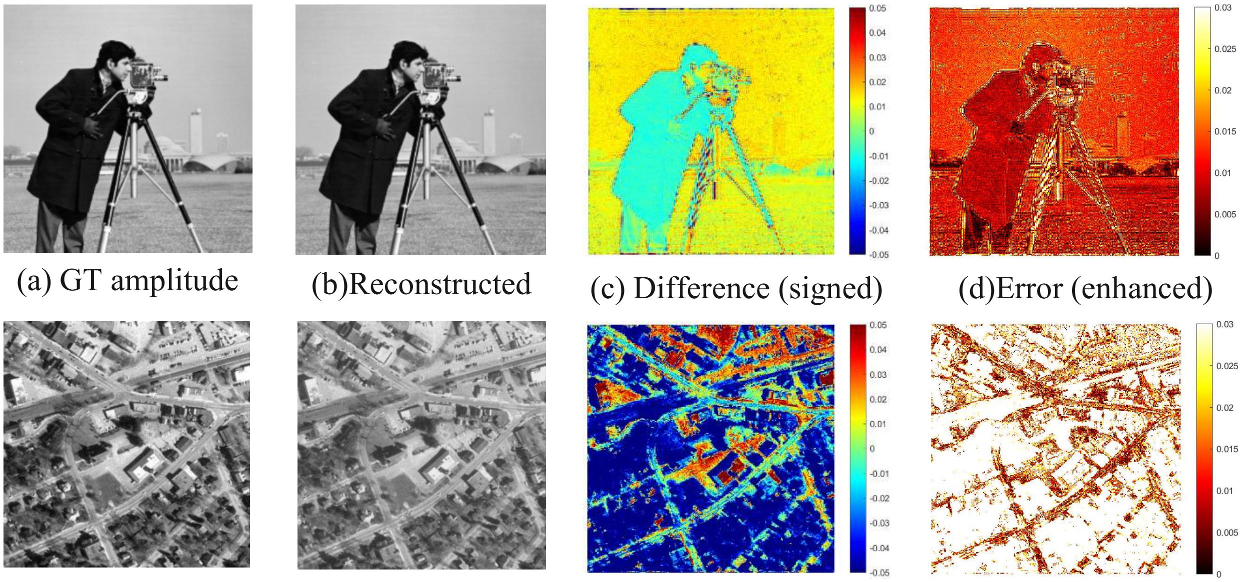

(a) GT amplitude (b)Reconstructed (c) Difference (signed) (d)Error (enhanced)

(e)GT phase (f)Reconstructed (g)Difference (signed) (h) Error (enhanced)

Figure 5. Visual comparison of reconstruction, difference, and error maps for amplitude and phase.

The signed difference maps (c, g) reveal directional deviation trends. Amplitude deviation remains symmetric with no global drift, while phase deviation slightly leans negative near object edges. The enhanced error maps (d, h) clearly highlight high-frequency regions and texture boundaries, showing that most residuals concentrate around structural transitions.

These results confirm that the proposed method offers high local accuracy in both amplitude and phase, preserves structural details, and effectively suppresses large-scale deviations.

4. Conclusion

In this study, we proposed a high-fidelity Fourier ptychographic reconstruction framework based on spiral-encoded LED illumination and adaptive multi-error feedback. By redesigning the illumination sequence and incorporating error-driven spectrum fusion, the proposed method improves phase-amplitude recovery accuracy and convergence stability with reduced iteration count.

A spiral illumination strategy was introduced to enhance frequency-domain uniformity and suppress peripheral degradation. Additionally, a multi-metric feedback mechanism incorporating amplitude error, phase error, and global residual was employed to guide spectrum updates throughout iterative reconstruction. The framework was validated through comprehensive simulations using 255 synthetic low-resolution images generated under a simulated 15×15 LED array setup.

Quantitative results demonstrate that the final amplitude reconstruction reaches a PSNR of 37.33 dB and SSIM of 0.9848, while the phase reconstruction achieves 24.18 dB and SSIM of 0.9384. Error maps and signed difference visualizations further reveal consistent structure preservation and local robustness. These findings confirm the effectiveness of the proposed method in simulation-based scenarios and lay a foundation for future physical implementation.

Acknowledgments

This work was supported by the Undergraduate Innovation Training Project of North China University of Science and Technology under Grant No. X2024030, titled “Design and

Implementation of a Fourier Ptychographic Microscopy System." The authors would like to sincerely thank Professor Yi Wang for his invaluable guidance throughout the research process.

References

[1] Zhang J, Xu T, Zhang J, Chen Y, Li J. Cross-level channel attention network for Fourier ptychographic microscopy reconstruction[J]. IEEE Photonics Journal, 2021, 14: 1–8.

[2] Sun M, Shao L, Zhu Y, Wang H, Liu Q. Double-flow convolutional neural network for rapid large field of view Fourier ptychographic reconstruction[J]. Journal of Biophotonics, 2021, 14(5): e202000444.

[3] Chen Q, Huang D, Chen R. Fourier ptychographic microscopy with untrained deep neural network priors[J]. Optics Express, 2022, 30(25): 39597–39612.

[4] Zhou G, Zhang S, Hu Y, Zhang J. Fast color Fourier ptychographic microscopy based on spatial filtering frequency fusion[J]. Optics and Laser Technology, 2024, 159: 108002.

[5] Wang Y, Wang Y, Li J, Wang X. Fourier ptychographic microscopy reconstruction method based on residual local mixture network[J]. Sensors, 2024, 24(13): 4099.

[6] Shu Y, Sun J, Lyu J, Jiang Y. Adaptive optical quantitative phase imaging based on annular illumination Fourier ptychographic microscopy[J]. PhotoniX, 2022, 3: 24.

[7] Zhou G, Zhang S, Hu Y, Yu Y. Fast digital refocusing in Fourier ptychographic microscopy based on defocus-distance regression network[J]. Optics Express, 2023, 31(1): 339–352.

[8] Liu H, Xu T, Chen Y, Liang Y. Transformed pupil-function misalignment calibration strategy for Fourier ptychographic microscopy[J]. Optics Express, 2024, 32(7): 11429–11446.

[9] Chen Y, Xu J, Pan A. Depth-of-field extended Fourier ptychographic microscopy without defocus distance priori[J]. Optics Letters, 2024, 49(11): 3222–3225.

[10] Feng T, Wang A, Wang Z, Sun M. Linear-space-variant model for Fourier ptychographic microscopy[J]. Optics Letters, 2024, 49(10): 2617–2620.

[11] Zhou G, Zhang S, Hu Y, Zhao C. Fast full-color pathological imaging using Fourier ptychographic microscopy via spatial filtering frequency fusion[J]. Advanced Photonics Nexus, 2025, 4(2): 026001.

[12] Zhang S, Berendschot T T J M, Zhou J. ELFPIE: an error-laxity Fourier ptychographic iterative engine[J]. arXiv preprint arXiv:2209.14671, 2022.

[13] Li H, Wei X, Liu Y, Wu Q. Fourier ptychographic microscopy based on spatial attention residual network for high-fidelity reconstruction[J]. Optics Express, 2022, 30(3): 3558–3573.

[14] Xie Z, He X, Sun X, Zhao Y. Spectral attention network for robust Fourier ptychographic reconstruction under noise[J]. Biomedical Optics Express, 2023, 14(1): 140–157.

[15] Wang J, Yuan S, Li K, Chen C. Deep learning-based denoising framework for Fourier ptychographic microscopy under low exposure conditions[J]. Journal of Biomedical Optics, 2022, 27(4): 046001.

[16] Huang D, Chen Q, Shen Y, Wang X. Physics-informed generative adversarial networks for super-resolution phase reconstruction in Fourier ptychographic microscopy[J]. Optics Communications, 2023, 532: 129161.

[17] Tang Z, Ye H, Han Q, Liu S. Fourier ptychographic imaging using frequency-enhanced neural networks[J]. Journal of Microscopy, 2023, 290(1): 14–25.

[18] Xu L, Zhang Y, Wang Z, Liu C. Fourier ptychographic microscopy based on image quality-aware adaptive data acquisition strategy[J]. Applied Optics, 2022, 61(23): 6815–6823.

[19] Jin L, Gao C, Li P, Liu Y. Fourier ptychographic imaging with a physical-model-constrained transformer network[J]. IEEE Transactions on Instrumentation and Measurement, 2024, 73: 1–10.

[20] Wang X, Sun J, Yang C, Zhao X. LED array misalignment calibration for Fourier ptychographic microscopy using simulated annealing optimization[J]. Applied Sciences, 2021, 11(14): 6542.

[21] Wang H, Tan Y, Liu J. Compressive Fourier ptychographic imaging with multi-scale adaptive frequency fusion[J]. Optical and Quantum Electronics, 2021, 53(11): 679.

[22] Qiu H, Zhang M, Wang F. Wide-field super-resolution phase imaging by deep neural networks in Fourier ptychographic microscopy[J]. Scientific Reports, 2021, 11: 15567.